PHYSICAL REVIEW A VOLUME 39, NUMBER 3 FEBRUARY 1, 1989

Angular distribution of ejected electrons in resonant Auger processes of Ar, Kr, and Xe

Thomas A. Carlson and David R. Mullins
Oak Ridge National Laboratory, Oak Ridge, Tennessee 37831-6201

Charles E. Beall, Brian W. Yates, and James W. Taylor
Department of Chemistry, University of Wisconsin, Madison, Wisconsin 53706

Dennis W. Lindle
National Bureau of Standards, Gaithersburg, Maryland 20899

Frederick A. Grimm
Department of Chemistry, University of Tennessee, Knoxville, Tennessee 37996-1600
(Received 25 May 1988)

Angle-resolved electron spectroscopy with the help of synchrotron radiation has been used to study resonant Auger processes near the core shells of Ar $2p$, Kr $3d$, and Xe $4d$. Results for the lowest-energy resonances have received special attention: argon ($Ar\ 2p_{3/2} \rightarrow 4s$) at a photon energy of 244.4 eV, krypton ($Kr\ 3d_{5/2} \rightarrow 5p$) at 91.2 eV, and xenon ($Xe\ 4d_{5/2} \rightarrow 6p$) at 65.1 eV. The angular distribution parameters β are evaluated for each of the resolved Auger peaks. Most striking is the occurrence of large negative β values for some of the higher kinetic energy peaks. The results are most apparent under high electron resolution. The theoretical basis for having β values near -1 is discussed. In particular, the experimental results for argon are found to be in general agreement with the prediction of -1 β values by using either angular momentum transfer theory or normal Auger theory. However, a better understanding of the range of β values will have to await explicit calculations. Experimental results on the Auger spectra are also given at lower kinetic energies, for shakeup states, and for higher-energy resonances, especially those involving vacancies in the core shells of the lower spin states. It is shown that, although transitions having the same final state of the singly charged ion frequently have similar relative intensities and β values, occasionally they differ quite markedly. The theoretical consequences of variant behavior for processes having the same final states are also discussed.

I. INTRODUCTION

A resonant Auger process will be defined in this paper as an Auger-like decay of an excited state produced by resonant photoabsorption in an inner shell. For example, at energies about 10 eV below the ionization potential of a core-shell electron, a photoabsorption resonance can occur to a virtual orbital. The excited neutral atom (or molecule) can then decay by an Auger process involving two valence-shell electrons, with the resultant filling of the core vacancy and ejection of an Auger electron. The excited electron can (1) remain in its orbital as a spectator electron, (2) be directly involved in the Auger process, or (3) be shaken up as the result of the Auger process to a still higher excited orbital or shaken off into the continuum. As one increases the photon energy, higher-energy resonances occur with the production of different Auger processes until the ionization potential is reached. Studies on resonant Auger processes are best carried out with the help of a storage ring emitting synchrotron radiation, which is intense, continuous, and sufficiently energetic to excite core-shell electrons.

There have been a number of investigations recently by resonant Auger processes, both on atomic[1-6] and molecular[7-11] systems. Relatively little attention, however, has been paid to the angular distribution of the ejected electrons.[6,9,11] It has not been until our present work on the rare gases in which angle-resolved electron spectrometry was employed with high resolution that unusually large anisotropy of ejected electrons was discovered. For example, in the angle-resolved spectrum[6] resulting from the resonance absorption of Kr to $(3d)^{-1}5p$ at a photon energy of 91.2 eV, there appear the final states $4p^4(^3P)5p(^4P_{5/2}$, $^4P_{3/2}$, and $^4D_{5/2})$ which give rise to angular distribution parameters, β, close to -1. The angular distribution parameter, β, is given[12] in terms of the differential cross section as

$$\frac{d\sigma}{d\Omega} = \frac{\sigma_{\text{tot}}}{4\pi}[1+\beta P_2(\cos\theta)] , \tag{1}$$

where P_2 is the Legendre polynomial of degree 2 in $\cos\theta$, and θ is the angle between the polarization vector and the direction of the ejected photoelectron or Auger electron. The value of β may range from $+2$ to -1. In the extreme limit of -1 no electrons are ejected parallel to the polarization vector.

In this paper we have continued our investigations[6] of the resonant Auger processes for the $3d$ core shell of Kr and extended them to Xe $4d$ and Ar $2p$. The studies have concentrated on the first resonances ($Kr:3d_{5/2} \rightarrow 5p$;

TABLE I. Resonant Auger processes for Kr $3d$.

Peak	Designation of final state	β	$I(\theta_m)$
	(a)		
	(See Fig. 1) $h\nu$=91.2 eV, $3d_{5/2}\rightarrow 5p$ (resolution: photon, 0.37 eV; electron 0.36 eV)		
1*a,b*	$4p^4(^3P)5p$	−0.45	23.4
1*c,d,e*	$4p^4(^3P)5p$	+0.66	43.0
2	$4p^4(^1D)5p$	+0.24	100.0
4	$4p^4(^1S)5p$	+0.73	62.9
5	$4p^4(^1D)6p$	−0.47	32.6
7	$4p^4(^1S)6p$	+0.34	20.2
	(b)		
	(See Ref. 6) $h\nu$=91.2 eV, $3d_{5/2}\rightarrow 5p$ (resolution: photon, 0.37 eV; electron, 0.12 eV)		
1*a*	$4p^4(^3P)5p\ ^4P_{5/2,3/2}$	−0.89(−0.87)[a]	20.7(19.1)[a]
1*b*	$4p^4(^3P)5p\ ^4P_{1/2},^4D_{7/2,5/2}$	−0.98(−1.02)	18.1(16.8)
1*c*	$4p^4(^3P)5p\ ^4D_{3/2},^2P_{1/2}$	+0.62(+0.71)	43.5(43.6)
1*d*	$4p^4(^3P)5p\ ^4D_{1/2},^2P_{3/2},^2D_{5/2}$	+0.24(+0.12)	26.8(11.6)
1*e*	$4p^4(^3P)5p\ ^2D_{3/2},^4S_{3/2},^2S_{1/2}$	+0.19(+0.28)	17.3(17.7)
2*a*	$4p^4(^1D)5p\ ^2F_{5/2,7/2},^2P_{3/2}$	−0.06(+0.05)	100.0(100.0)
2*b*	$4p^4(^1D)5p\ ^2P_{1/2},^2D_{3/2,5/2}$	−0.12(+0.06)	80.1(85.9)
	(c)		
	(See Fig. 3) $h\nu$=92.4 eV, $3d_{3/2}\rightarrow 5p$ (resolution: photon, 0.37 eV; electron 0.36 eV)		
1*a,b*	$4p^4(^3P)5p$	−0.30	13.3
1*c,d,e*	$4p^4(^3P)5p$	+0.10	23.2
2	$4p^4(^1D)5p$	−0.12	100.0
4	$4p^4(^1S)5p$	+0.82	62.9
5	$4p^4(^1D)6p$	−0.18	39.1
7	$4p^4(^1S)6p$	+0.28	26.0
	(d)		
	[See Fig. 2(a)] $h\nu$=91.2 eV, $3d_{5/2}\rightarrow 5p$ (resolution: photon, 0.37 eV; electron 0.24 eV)		
1*a*	$4p^4(^3P)5p\ ^4P_{5/2,3/2}$	−0.73(−0.91)[a]	22.3(21.6)[a]
1*b*	$4p^4(^3P)5p\ ^4P_{1/2},^4D_{7/2,5/2}$	−0.11(−0.32)	23.2(14.3)
1*c*	$4p^4(^3P)5p\ ^4D_{3/2},^2P_{1/2}$	+0.35(+0.45)	48.8(51.4)
1*d*	$4p^4(^3P)5p\ ^4D_{1/2},^2P_{3/2},^2D_{5/2}$	+0.59(+0.43)	29.7(3.7)
1*e*	$4p^4(^3P)5p\ ^2D_{3/2},^4S_{3/2},^2S_{1/2}$	+0.31(+0.57)	20.8(21.3)
2*a*	$4p^4(^1D)5p\ ^2F_{5/2,7/2},^2P_{3/2}$	0.00(+0.04)	100.0(100.0)
2*b*	$4p^4(^1D)5p\ ^2P_{1/2},^2D_{3/2,5/2}$	+0.10(+0.26)	86.3(97.6)
4	$4p^4(^1S)5p$	+0.46	77.2
5	$4p^4(^1D)6p$	−0.60	53.0
	(e)		
	[See Fig. 2(b)] $h\nu$=92.4 eV, $3d_{3/2}\rightarrow 5p$ (resolution: photon, 0.37 eV, electron 0.24 eV)		
1*a*	$4p^4(^3P)5p\ ^4P_{5/2,3/2}$	−0.48(−0.58)[a]	23.8(19.2)[a]
1*b*	$4p^4(^3P)5p\ ^4P_{1/2},^4D_{7/2,5/2}$	−0.20(−0.34)	11.1(4.0)
1*c*	$4p^4(^3P)5p\ ^4D_{3/2},^2P_{1/2}$	+0.46(−0.13)	19.1(9.9)
1*d*	$4p^4(^3P)5p\ ^4D_{1/2},^2P_{3/2},^2D_{5/2}$	+0.14(−0.16)	36.0(22.7)
1*e*	$4p^4(^3P)5p\ ^2D_{3/2},^4S_{3/2},^2S_{1/2}$	−0.26(−0.03)	28.4(14.9)
2*a*	$4p^4(^1D)5p\ ^2F_{5/2,7/2},^2P_{3/2}$	−0.16(−0.19)	100.0(100.0)
2*b*	$4p^4(^1D)5p\ ^2P_{1/2},^2D_{3/2,5/2}$	+0.08(+0.34)	104.0(83.6)
4	$4p^4(^1S)5p$	+0.49	109.2
5	$4p^4(^1D)6p$	−0.57	54.7
	(f)		
	(Lower kinetic-energy processes)		
	[See Fig. 4(a)] $h\nu$=91.2 eV, $3d_{5/2}\rightarrow 5p$ (resolution: photon, 0.37 eV; electron 0.36 eV)		
1	$4s^14p^5(^3P)5p$	+0.55	31.9
2	$4s^14p^5(^1P)5p$	+0.60	100.0
3	$4s^14p^5(^1P)6p$	+0.26	32.0
5	$4s^24p^34d(^1P)5p$	+0.33	52.2
6	$4s^24p^34d(^1P)6p$	+0.34	19.9
8	$4s^0(^0S)5p$	+0.83	48.9

TABLE I. (*Continued.*)

Peak	Designation final state	β	$I(\theta_m)$
	(g)		
	(Lower kinetic-energy processes)		
	[See Fig. 4(b)] $h\nu=92.4$ eV, $3d_{3/2}\rightarrow 5p$ (resolution: photon, 0.37 eV; electron 0.24 eV)		
2	$4s^1 4p^5(^1P)5p$	+0.52	100.0
3	$4s^1 4p^5(^1P)6p$	+0.30	56.6
4	?	+0.39	37.8
5	$4s^2 4p^3 4d^1(^1P)5p$	−0.02	34.0
6	$4s^2 4p^3 4d^1(^1P)6p$	+0.48	40.3
7	?	+0.29	37.0
8	$4s^0(^0S)5p$	+0.53	48.7
	(h)		
	(Normal Auger)		
	$h\nu=180$ eV (resolution: photon 0.37 eV, electron 0.36 eV)		
1	$(3d_{3/2})^{-1}\rightarrow 4p^4(^3P_2)$	−0.32	19.2
2	$(3d_{3/2})^{-1}\rightarrow 4p^4(^3P_{0,1})$	0.00	32.9
3	$(3d_{5/2})^{-1}\rightarrow 4p^4(^3P_2)$	−0.03	68.0
4	$(3d_{3/2})^{-1}\rightarrow 4p^4(^1D_2);3d_{5/2}\rightarrow 4p^4(^3P_{0,1})$	+0.15	117.1
5	$(3d_{5/2})^{-1}\rightarrow 4p^4(^1D_2)$	−0.11	104.7
6	$(3d_{3/2})^{-1}\rightarrow 4p^4(^1S_0)$	+0.22	70.0
7	$(3d_{5/2})^{-1}\rightarrow 4p^4(^1S_0)$	+0.24	77.7

[a]Values of β and $I(\theta_m)$ given in parentheses have been obtained from a deconvolution program.

Xe:$4d_{5/2}\rightarrow 6p$;Ar:$2p_{3/2}\rightarrow 4s$), but effects of the higher resonances have also been measured, particularly those involving the more tightly bound spin-orbit–split-core levels. Most of the final states that are reached can be described with one-electron configurations that leave the spectator electron in the excited orbital. In addition, some transitions involving electron shakeup are investigated. A wide variety of β values was observed, but the

TABLE II. Parity (un)favored transitions for the states of Kr, Xe, and Ar. For *jj* coupling only the total angular momentum need be specified, the value of the total electron spin and total orbital angular momentum does not change the results. Thus the $^4P_{3/2}$, $^2P_{3/2}$, $^4D_{3/2}$, etc., all have the same results, as indicated in the table for $J=\frac{3}{2}$. For *LS* coupling only the doublet states are allowed since the ejected electron has spin $\frac{1}{2}$ and the spin is zero for the ground state neutral. Thus the spin of the ion $S_c=0+\frac{1}{2}=\frac{1}{2}$.

Ion states total angular momentum, J	jt	Allowed $jt=l+1$	Favored	Unfavored
jj coupling: For Kr and Xe with electron configurations of $np^4(n')p$				
$\frac{7}{2}$	3,4	3	3	
$\frac{5}{2}$	2,3	2,3	3	2
$\frac{3}{2}$	1,2	1,2	1	2
$\frac{1}{2}$	0,1	1	1	0
For Ar with electron configurations $np^4(n')s$				
$\frac{7}{2}$	3,4	3		3
$\frac{5}{2}$	2,3	2,3	2	3
$\frac{3}{2}$	1,2	1,2	2	1
$\frac{1}{2}$	0,1	1		1
LS coupling: For selected states of Ar with electron configuration $np^4(n')s$				
^2P	1	1		1
^2D	2	2	2	
^2S	0			

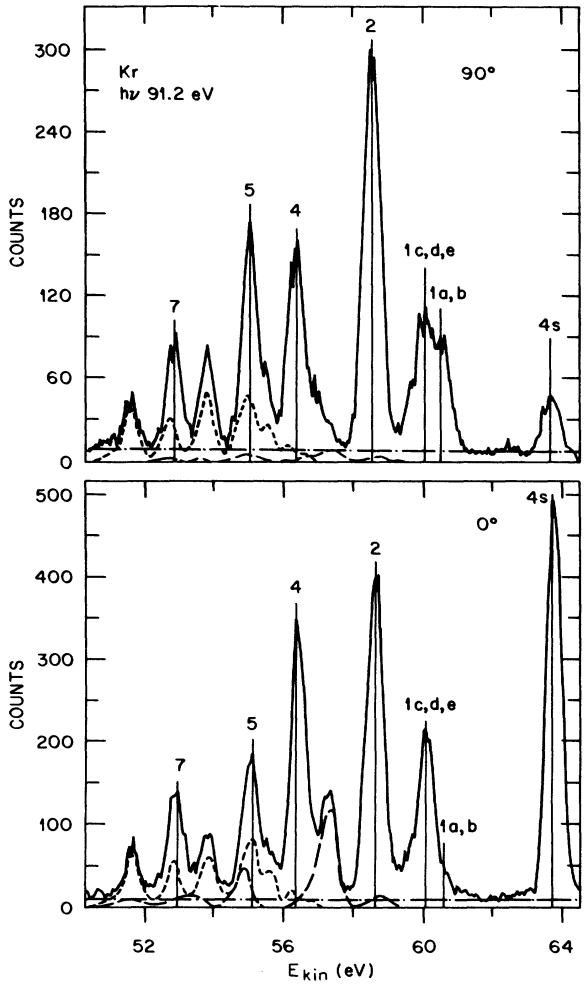

FIG. 1. Electron spectra for krypton measured at a photon energy of 91.2 eV. The kinetic-energy scale is given in eV. The long vertical lines mark the positions where intensities are measured. See Table I(a) for results of analyses and designation of numbered peaks. The 4s photoelectron peak is so indicated in the figure. Spectra have been taken at $\theta=90°$ (upper) and 0° (lower). The spectra are given by solid lines and the background by dashed lines: general background, dot dash; satellite structure, long dash; and normal Auger spectra, short dash. The resolution of the photon source is 0.37 eV FWHM, and that of the electron spectrometer at 90° is 0.36 eV FWHM.

most interesting are the highly negative values near -1, which have been seen for Xe and Ar as well as Kr.

The resonant Auger process is an autoionization process involving core excited states. Thus the theories of autoionization usually used for autoionization involving valence electrons should be appropriate for the resonant Auger process provided any approximations used include the characteristics of core excited states. An understanding of the autoionization process would require explicit calculations in order to determine the relative importance of the various channels in the ionization process. Thus it was tempting to try a qualitative approach to understand the near -1 β values obtained for certain transitions. Two approaches readily come to mind. The first is to use angular momentum transfer theory.[13] Results from this theoretical treatment will be made for specific cases pertinent to the experimental results discussed in this paper. As will be seen, our use of this approach suffers from its dependence on the one-electron model. In addition, only initial and final states using either *LS* or *jj* coupling are considered, rather than a more appropriate intermediate coupling. The second approach is to use the alignment parameter from the theories of the normal Auger process.[14,15] Plane-polarized radiation leads to an alignment of the resonant state in *LS* coupling. We have not completely investigated the use of this model. The alignment parameter A_{20} can easily be obtained for the case of argon using *LS* coupling. The value of $-\sqrt{2}$ is predicted for photoexcitation of the $2p_{3/2}^{-1}(^2P_{3/2})4s\ ^1P_1$ with linear-polarized synchrotron radiation. Using the formalism for Auger electrons we have $\beta=A_{20}\alpha_2$, where α_2 depends on the final state.[16] Thus different β values are obtained depending on the value of α_2. Indeed, a -1 β value is obtained for the decay $2p_{3/2}^{-1}4s\ ^1P_1 \rightarrow 3p^{-2}(^3P)4s(^2P_{1/2,3/2})$. The second approach is very appealing and gives justification of the negative β value for the one final state in argon which shows a large negative β value. However, it also suffers from the use of either *LS* or *jj* coupling rather than the appropriate intermediate coupling. The mixing that occurs with the use of intermediate coupling will require calculations to determine the important contributions to the cross section and angular distributions.

The principal aim of this paper is to characterize the photoelectron dynamics of the angular distribution of ejected electrons in the resonant Auger process. However, the data can also be used to help identify the final state of the singly charged ions, which can help complement data from optical spectroscopy.

II. EXPERIMENTAL PROCEDURE

The experiment consists of measuring both Auger and photoelectron spectra of the rare-gas atoms as a function of photon energy and emission angle. The experimental chamber has been described before.[11,17] It consists of three spherical sector analyzers mounted on a rotatable platform located perpendicular to the direction of the incoming photon beam emitted from a synchrotron light source. The photon source was the Aladdin Storage Ring operated by the University of Wisconsin at Stoughton. The monochromator used is owned by the Synchrotron Radiation Center. It is designated the Mark V, is of the grasshopper design, and contains a two-meter grating. In this experiment, the resolution of the monochromator was varied from 0.27 to 0.54 Å.

After calibrating the performance of the electron spectrometer against values of β given in the literature[18] for rare gases and by checking the $\cos^2\theta$ dependence by rotating the platform, the runs were taken with two of the spectrometers that were mounted at right angles to each other. One spectrometer received electrons parallel to

TABLE III. Resonant Auger processes for Xe $4d$.

Peak	Designation of final state	β	$I(\theta_m)$
	(a)		
	(See Fig. 5) $h\nu=65.1$, $4d_{5/2}\rightarrow 6p$ (resolution: photon, 0.19 eV; electron 0.36 eV)		
$1a,b$	$5p^4(^3P)6p$	-0.67	46.1
$1c$	$5p^4(^3P)6p$	$+1.09$	59.9
2	$5p^4(^3P)6p$	$+0.48$	45.9
3	$5p^4(^1D)6p$	$+0.12$	100.0
5	$5p^4(^1S)6p, 5p^4(^1D)7p$	$+0.51$	81.2
6	$5p^4(^1D)7p$	-0.03	26.6
8	?	$+0.79$	20.3
	(b)		
	(See Fig. 6) $h\nu=65.1$ eV, $4d_{5/2}\rightarrow 6p$ (resolution: photon, 0.19 eV; electron 0.12 eV)		
$1a$	$5p^4(^3P)6p\ ^4P_{5/2,3/2}$	$-0.88(-0.80)$[a]	19.0(15.2)[a]
$1b$	$5p^4(^3P)6p\ ^4P_{1/2}[^2P_{1/2}], ^4D_{7/2}, ^4D_{5/2}[^2D_{5/2}]$	$-0.93(-1.02)$	42.3(37.4)
$1c$	$5p^4(^3P)6p\ ^4D_{3/2}[^2P_{3/2}]$	$+0.82(+1.11)$	52.3(57.5)
$2a$	$5p^4(^3P)6p\ ^4D_{1/2}, ^2S_{1/2}[^4P_{1/2}], ^4S_{3/2}[^4D_{3/2}]$	$+0.26(+0.39)$	31.4(28.9)
$2b$	$5p^4(^3P)6p\ ^2D_{5/2}[^4D_{5/2}], ^2D_{3/2}, ^2P_{3/2}[^4S_{3/2}], ^2P_{1/2}[^2S_{1/2}]$	$+0.16(+0.19)$	32.1(30.3)
$3a$	$5p^4(^1D)6p\ ^2F_{5/2,7/2}, ^2P_{3/2}$	$-0.02(+0.14)$	67.9(65.3)
$3b$	$5p^4(^1D)6p\ ^2P_{1/2}, ^2D_{3/2,5/2}$	$-0.09(+0.07)$	100.0(100.0)
	Designation of final state taken from Moore, Ref. 20. Alternative designation given in brackets from Ref. 24.		
	(c)		
	(See Fig. 8) $h\nu=67.0$ eV, $4d_{3/2}\rightarrow 6p$ (resolution: photon, 0.19 eV; electron 0.36 eV)		
$1a,b$	$5p^4(^3P)6p$	-0.67	12.9
$1c$	$5p^4(^3P)6p$	-0.38	4.7
2	$5p^4(^3P)6p$	$+0.14$	36.1
3	$5p^4(^1D)6p$	$+0.32$	100.0
5	$5p^4(^1S)6p, 5p^4(^1D)7p$	$+0.89$	96.0
6	$5p^4(^1D)7p$	-0.29	37.3
	(d)		
	(Lower kinetic-energy processes)		
	[See Fig. 9(a)] $h\nu=65.1$ eV $4d_{5/2}\rightarrow 6p$ (resolution: photon, 0.19 eV; electron 0.36 eV)		
1	$5s^15p^5(^1P,^3P)6p$	$+1.37$	14.2
2	$5s^15p^5(^1P,^3P)6p$	$+0.62$	100.0
3	$5s^15p^1(^1P,^3P)7p$	$+0.29$	52.6
4	$5s^15p^5(^1P,^3P)7p$	$+0.53$	131.1
	Designation of final state not well established		
	(e)		
	[See Fig. 9(b)] $h\nu=67.0$ eV, $4d_{3/2}\rightarrow 6p$ (resolution: photon, 0.19 eV; electron 0.36 eV)		
1	$5s^15p^5(^1P,^3P)6p$	$+1.55$	14.8
2	$5s^15p^5(^1P,^3P)6p$	$+0.97$	100.0
3	$5s^55p^5(^1P,^3P)7p$	$+0.63$	67.5
4	$5s^15p^5(^1P,^3P)7p$	$+0.51$	108.0
	Designation of final state not well established		
	(f)		
	Normal Auger		
	$h\nu=74.8$ eV (resolution: photon, 0.19 eV; electron 0.36 eV)		
1	$4d_{3/2}\rightarrow 4p^4(^3P_2)$	-0.06	5.8
2	$4d_{3/2}\rightarrow 4p^4(^3P_1)$	$+0.10$	23.0
3	$4d_{3/2}\rightarrow 4p^4(^1D_2)4d_{5/2}\rightarrow 4p^4(^3P_2)$	$+0.10$	100.0
4	$4d_{5/2}\rightarrow 4p^4(^3P_{1,0})$	$+0.20$	43.4
5	$4d_{3/2}\rightarrow 4p^4(^1S_0)4d_{5/2}\rightarrow 4p^4(^1D_2)$	-0.05	83.8
6	$4d_{5/3}\rightarrow 4p^4(^1S_0)$	$+0.27$	45.4

TABLE III. (*Continued.*)

Peak	Designation of final state	β	$I(\theta_m)$
	(g) (Normal Auger, low kinetic energy) $h\nu=130$ eV (resolution: photon, 0.19 eV; electron 0.36 eV)		
1,2′	$(4d_{3/2})^{-1},(4d_{5/2})^{-1}\rightarrow 5s^1 5p^5 \rightleftarrows 5s^2 5p^3 5d^1, 6s^1$	+0.05	44.7
2	$(4d_{3/2})^{-1},(4d_{5/2})^{-1}\rightarrow 5s^1 5p^5 \rightleftarrows 5s^2 5p^3 5d^1 6s^1$	+0.09	63.9
3′	$(4d_{3/2})^{-1},(4d_{5/2})^{-1}\rightarrow 5s^1 5p^5 \rightleftarrows 5s^2 5p^3 5d^1, 6s^1$	+0.17	29.3
4′	$(4d_{3/2})^{-1},(4d_{5/2})^{-1}\rightarrow 5s^1 5p^5 \rightleftarrows 5s^2 5p^3 5d^1, 6s^1$	+0.07	72.7
3	$(4d_{3/2})^{-1},(4d_{5/2})^{-1}\rightarrow 5s^1 5p^5 \rightleftarrows 5s^2 5p^3 5d^1, 6s^1$	+0.13	52.7
4	$(4d_{3/2})^{-1},(4d_{5/2})^{-1}\rightarrow 5s^1 5p^5 \rightleftarrows 5s^2 5p^3 5d^1, 6s^1$	+0.06	100.0

[a]Values of β and $I(\theta_m)$ given in parentheses have been obtained from a deconvolution program.

the polarization vector, while the other analyzed electrons emitted perpendicular to the polarization vector. The electron-energy spectrum was swept by varying the accelerating or decelerating voltage. The angular distribution parameter β is derived[17] from the expression

$$\beta=\frac{4(R-1)}{3P(R+1)-(R-1)}\ , \tag{2}$$

where P is the degree of polarization and R is $I(0°)/I(90°)$. $I(0°)$ and $I(90°)$ are the measured intensities of the ejected electrons moving in the direction parallel or perpendicular to the polarization vector. Studies of near-zero β values as derived from the literature[18] were used to check isotropic distribution and high-β values to experimentally ascertain the polarization. The relative efficiencies and resolution of the two spectrometers were

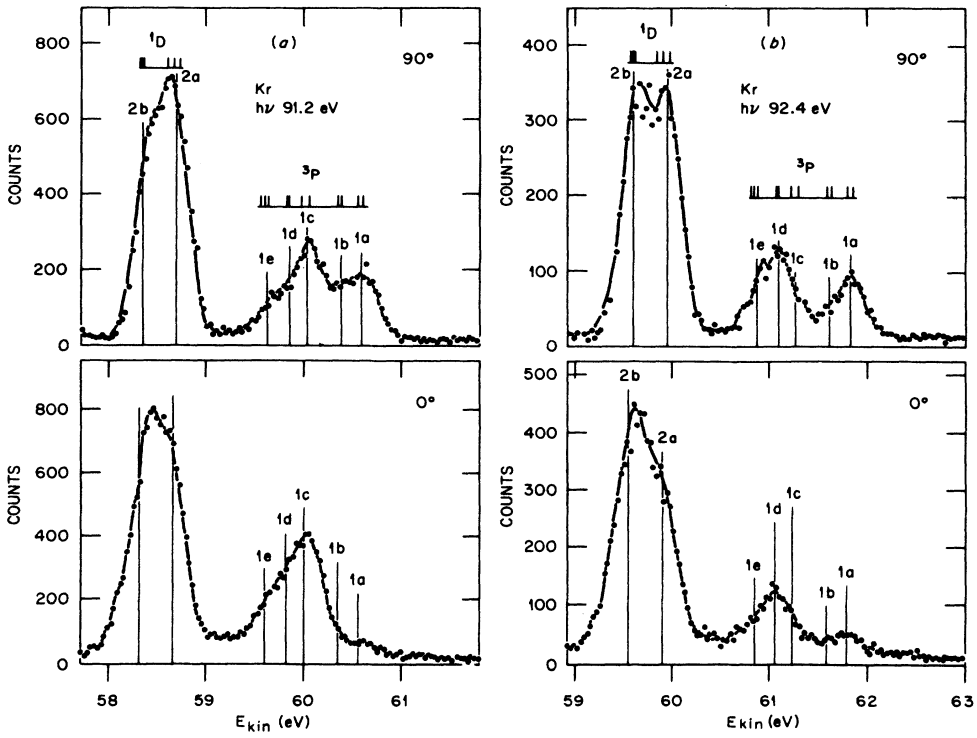

FIG. 2. Comparison of the higher kinetic-energy portion of the electron spectra for krypton measured at photon energies of (a) 91.2 and (b) 92.4 eV. The long vertical lines mark the positions where the intensities are measured. See Tables I(d) and I(e) for results of analyses and designation of numbered peaks. The short vertical lines, which indicate possible positions of Auger peaks, are derived from optical data (Ref. 20). Spectra have been taken at $\theta=90°$ (upper) and 0° (lower) and are drawn as solid lines. The kinetic-energy scale is given in eV. The resolution of the photon source is 0.37 FWHM and that of the electron spectrometer at 90° is 0.24 eV FWHM.

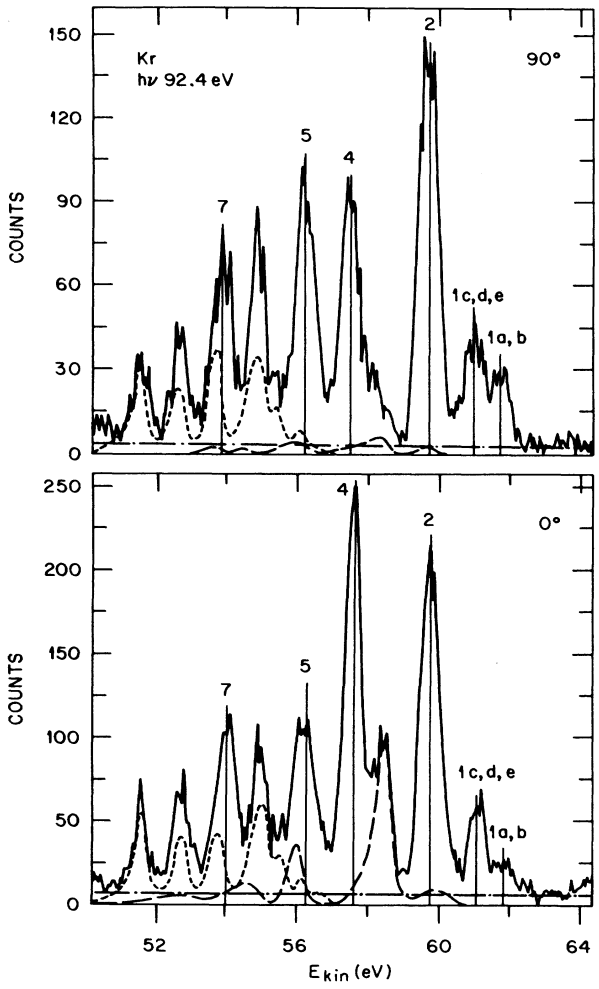

FIG. 3. Electron spectra for krypton measured at a photon energy of 92.4 eV. The kinetic-energy scale is given in eV. The long vertical lines mark the positions where the intensities are measured. See Table I(c) for results of analyses and designation of numbered peaks. Spectra have been taken at $\theta=90°$ (upper) and 0° (lower). The spectra are given by solid lines and the background by dashed lines: general background, dot dash; satellite structure, long dash; and normal auger spectra, short dash. The resolution of the photon source is 0.37 eV FWHM and that of the electron spectrometer at 90° is 0.36 eV FWHM.

also determined and used to correct the data. The resolution of the spectrometers are proportional to the band-pass energy. The resolution of the spectrometer usually used to measure spectra at 90° was 1.2% of the pass energy, while that used to measure spectra at 0° was 1.8%. In the runs described in this paper the degree of polarization was found to be 0.815.

The angle-integrated intensities are obtained[12] from the intensity at the magic angle for a given polarization

$$I(\theta_m)=I(0°)\frac{1}{1+[\beta(1+3P)/4]} . \quad (3)$$

The β values and intensities are derived from the values of the spectral intensities, usually at the peaks, after correction for background. Since the spectra are derived from a large number of partially resolved or unresolved final states, the analysis is dependent on the resolution of the electron analyzers. In appropriate cases where higher resolution was used with reasonably good counting statistics, we have also carried out analyses using a computer fitting program.

III. RESULTS AND DISCUSSION

A. Kr 3*d*

An interpretation of the photoabsorption spectrum of Kr just below the ionization potential for the $3d_{5/2}$ and $3d_{3/2}$ core shells can be found in the literature.[19] From these studies the following results should be noted. The lowest resonance energy for promoting an electron out of the 3*d* core shell of Kr occurs at 91.20 eV representing the transition $3d_{5/2}\rightarrow 5p$. It is well separated in energy from subsequent resonances. The next-higher-energy resonances occur at 92.43 eV ($3d_{3/2}\rightarrow 5p$) and at 92.56 eV ($3d_{5/2}\rightarrow 6p$). The relative oscillator strengths for the first three resonances are, respectively, 1.0, 0.63, and 0.37. Higher-energy resonances in the Rydberg series, which were not examined in our present studies, lead to the ionization potentials for the $3d_{5/2}$ and $3d_{3/2}$ subshells of 92.79 and 95.04 eV, respectively.

1. Kr: First resonance ($3d_{5/2}\rightarrow 5p$)

Results from the study of the resonance Auger processes for the first resonance in Kr (91.2 eV) are given in Tables I(a), I(b), and I(d) and Figs. 1 and 2(a). The designations have been made first from the energy spacings obtainable from optical data[20] for singly charge krypton. These are available for all possible states for the configuration $4p^4 5p$, and the results fit the experimental data quite well. [See Figs. 1 and 2(a) and the figure with the higher-resolution data in Ref. 6.] In addition, use has been made of the analysis by Aksela *et al.*[1] of the resonant Auger processes in Kr. Their study reported on similar measurements to those given in this paper, but their measurements were carried out only at the magic angle. Our data make an ideal complement to theirs. We have used the same number scheme as Aksela *et al.*[1] to identify the observed peaks. Their designations are based largely on relativistic multiconfiguration calculations for the transition energies. In cases where we have resolved additional structure due to higher electron resolution the numbers have been broken down into subsets carrying a letter subscript.

In Fig. 1 and in subsequent figures, three backgrounds are indicated. One is general background from counter noise, scattered electrons, etc. The second results from "normal" Auger processes, that is, from nonresonant processes in which a core electron (actually from either the $3d_{5/2}$ or $3d_{3/2}$ subshell) is removed directly into the continuum. Because the monochromator passes some higher-order radiation with wavelengths $1/n$ times that

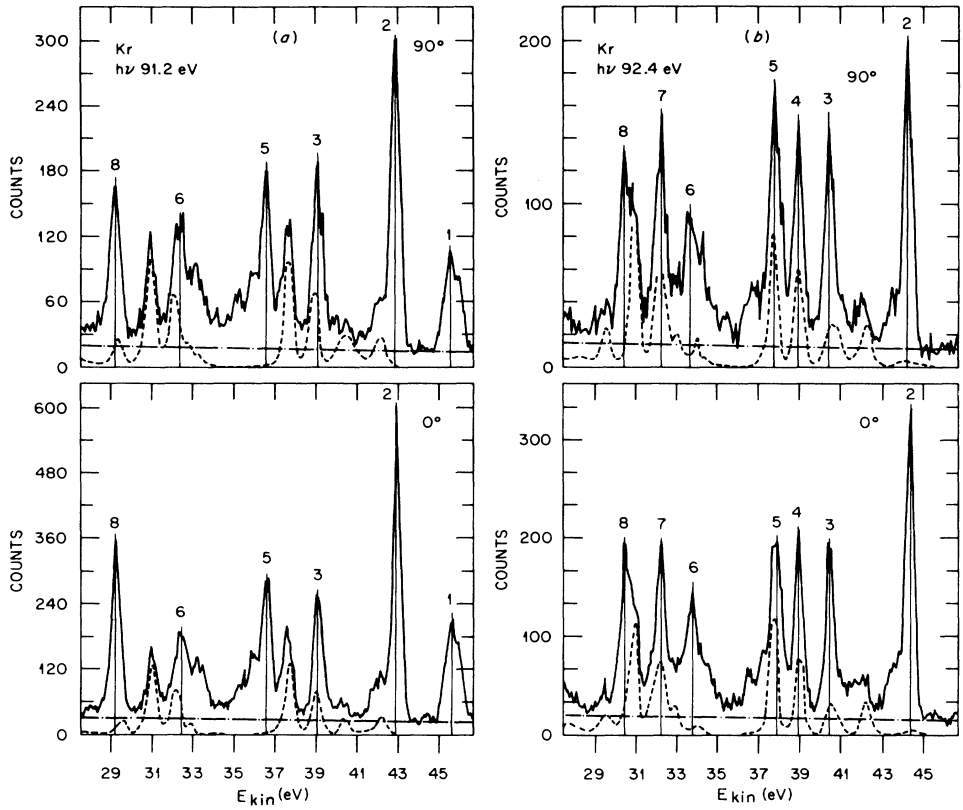

FIG. 4. Comparison of the lower kinetic-energy portion of the electron spectra for krypton measured at photon energies (a) 9.12 and at (b) 92.4 eV. The long vertical lines mark the positions where intensities are measured. See Tables I(f) and I(g) for results of analyses and designation of numbered peaks. Spectra have been taken at $\theta=90°$ (upper) and 0° (lower) and are drawn as solid lines. The backgrounds are given by dashed lines: general background, dot dash; normal Auger spectra, short dash. The kinetic-energy scale is given in eV. The resolution of the photon source is 0.37 eV FWHM and that of the electron spectrometer at 90° is 0.36 eV FWHM.

of the dominant first-order radiation, some contamination can arise from the normal Auger processes created by high-energy photons. The Kr and Xe studies are particularly plagued since photons with twice the energy needed to excite the resonances are in a region of fairly high photoabsorption cross section for the d core shells. By studying the normal Auger-electron spectrum off-resonance one is able to obtain a fairly accurate correction. The third background comes from direct photoelectron processes from the valence shell. The main lines do not interfere, but some of the satellite structure does. It too can be corrected from data taken off resonance, on the assumption that the relative cross sections for photoionization vary only slightly with energy in the region being studied. The assumption is valid, except where one might conceive of channel interaction processes at the resonances. We believe that, in general, our analysis is not affected, but in any case, the backgrounds shown in the figures are reliable for nonresonant behavior.

On examining the data in Fig. 1 and Tables I(a) and I(b), it is clear that the angular distribution parameters β vary considerably according to the particular transitions. Striking cases are the two highest-energy peaks, 1a and 1b, particularly under higher-electron energy resolution, where the β values were measured to be, respectively, -0.89 and -0.98. These extreme values suggest some selection rule is in force. For example, using angular momentum transfer theory as formulated by Fano and Dill[13] the matrix elements responsible for negative-β values can be identified using either LS or jj coupling. Values of β near -1 also have been observed in the autoionization of the valence shells of atoms and discussed in the context of the angular momentum transfer theory.[21] There are important differences, however, between resonances initiated in the core shell and those arising from the valence shell. First, the energy of the Auger electrons arising from a core-shell vacancy are much larger than those resulting from valence-shell excitation. Even more important, core-shell excitation allows for a spectator electron decay which is usually not energetically possible for the valence shell. Valence-shell autoionization usually proceeds through a direct participation of the excited electrons.

In applying the angular-momentum transfer theory, one considers the original state of the neutral atom and the final state of the ion after ionization but not the de-

TABLE IV. Resonant Auger processes for Ar $2p$

Peak	Designation of final state	β	$I(\theta_m)$
	(a)		
	(See Fig. 10) $h\nu=244.4$ eV, $2p_{3/2}\rightarrow 4s$ (resolution: photon, 1.30 eV; electron 0.60 eV)		
1	$3p^4(^3P)4s$	−0.53	84.0
2	$3p^4(^1D)4s$	+0.36	100.0
3	$3p^4(^1S)4s$	+0.39	28.3
4	$3p^4(^3P)5s$	−0.03	24.0
5	$3p^4(^1D)5s$	−0.05	17.5
	(b)		
	(See Fig. 10) $h\nu=244.4$ eV, $2p_{3/2}\rightarrow 4s$ (resolution: photon, 1.82 eV; electron 0.36 eV)		
1*a*	$3p^4(^3P)4s\ ^4P_{5/2,3/2,1/2}$	+0.23(+0.37)[a]	53.5(20.1)[a]
1*b*	$3p^4(^3P)4s\ ^2P_{3/2,1/2}$	−0.69(−0.86)	70.9(96.1)
2	$3p^4(^1D)4s\ ^2D_{3/2,5/2}$	+0.48(+0.45)	100.0(100.0)
3	$3p^4(^1S)4s\ ^2S_{1/2}$	+0.66	36.0
	(c)		
	(See Fig. 11) $h\nu=246.5$ eV $2p_{3/2}\rightarrow 3d$ (resolution: photon, 1.30 eV; electron 0.60 eV) $2p_{1/2}\rightarrow 4s$		
1*a*	$(2p_{1/2})^{-1}4s\rightarrow 3p^4(^3P)4s\ ^4P_{5/2,3/2,1/2}$	+0.10	43.9
1*b*	$(2p_{1/2})^{-1}4s\rightarrow 3p^4(^3P)4s\ ^2P_{3/2,1/2}$	−0.37	61.1
2	$(2p_{1/2})^{-1}4s\rightarrow 3p^4(^1D)4s$	−0.22	100.0
3	$(2p_{3/2})^{-1}3d\rightarrow 3p^4(^1D)3d$	−0.44	198.2
4	$(2p_{3/2})^{-1}3d\rightarrow 3p^4(^3P)4d$	−0.09	134.4
5	$(2p_{3/2})^{-1}3d\rightarrow 3p^4(^1D)4d$	−0.23	195.7
6	$(2p_{3/2})^{-1}3d\rightarrow 3p^4(^1S)4d$	+0.14	81.1
	(d) (Normal Auger) $h\nu=267$ eV (resolution: photon, 1.30 eV; electron 0.60 eV)		
1	$(2p_{1/2})^{-1}\rightarrow 3p^4(^3P)$	+0.21	20.5
2	$(2p_{1/2})^{-1}\rightarrow 3p^4(^1D);(2p_{3/2})^{-1}\rightarrow 3p^4(^3P)$	+0.02	87.4
3	$(2p_{1/2})^{-1}\rightarrow 3p^4(^1S);(2p_{3/2})^{-1}\rightarrow 3p^4(^1D)$	−0.17	100.0
4	$(2p_{3/2})^{-1}\rightarrow 3p^4(^1S)$	−0.02	33.1

[a]Values of β and $I(\theta_m)$ given in parentheses have been obtained from a deconvolution program.

tailed dynamics of the resonant state. The criteria for a favored or unfavored transition based on the angular-momentum transfer theory are

$$(-1)^{j_t}=\Pi_0\Pi_c \text{ for favored transitions} \quad (4a)$$

$$=-\Pi_0\Pi_c \text{ for unfavored transitions}, \quad (4b)$$

where Π_0 is the total parity of the original state of the atom, which for the ground state of the rare gases is $+1$, and Π_c is the total parity of the final state of the ion. For unfavored transitions $\beta=-1$; for favored transitions β can take any value for $+2$ to -1. The angular momentum transfer j_t is equal to $J_c+\frac{1}{2}$, for jj coupling with our restrictions.[22] A list of the results for the systems studied is summarized in Table II. To help force the theory to yield some specific predictions, we have also assumed[23] the single-electron selection rule: $j_t=l\pm 1$. For ionization of an electron in a p orbital, l can have the values 0 or 2. For the lighter element Ar we also show the results for LS coupling, where $j_t=L_c$. The $\Delta S=0$ rule allows only doublet states. We shall use jj coupling for Kr and Xe, and use the LS results only for Ar.

The peak 1a of Kr [see Table I(b)] is found to include contributions from two final states: $4p^4(^3P)5p\ ^4P_{5/2}$ and $^4P_{3/2}$. These quartet states would not be allowed within LS coupling. With jj coupling there are parity-favored and parity-unfavored terms for both states. The large negative β values observed experimentally can be explained, if the parity-unfavored term dominates the transition due to the influence of the resonant state. For the penultimate band, 1*b*, three final states can contribute: $^4P_{1/2}$, $^4D_{7/2}$, and $^4D_{5/2}$. Only the $^4D_{5/2}$ state contains a parity-unfavored term, which would suggest that the value of β for this peak can be explained only if the parity-unfavored $^4D_{5/2}$ state dominates the transition. (The $^4D_{7/2}$ can have a parity-unfavored term if one includes kg continuum channels.)

In surveying the data of the first resonance [Fig. 1, Table I(a)] one might also note a high positive β associated with the ^1S core term value (peak 4) and the large negative value for peak 5 [a shakeup transition to the $4p^4(^1D)\ 6p$ state].

2. Kr: Second resonance ($3d_{3/2} \rightarrow 5p$)

Results for the second resonance are found in Tables I(c) and I(e) and Figs. 2 and 3. These results should be closely compared with those of the first resonance since they both give rise to the same final states. The kinetic energies of the resonant Auger electrons for the second resonance are displaced upward by exactly the difference in resonance energies (1.23 eV). Comparing the β values and relative intensities [Fig. 1 versus Fig. 3 and Table I(a) versus I(c)] for the lower-resolution (0.36 eV) data, we find strong resemblances. A more detailed study of the higher kinetic-energy bands, Fig. 2 [Table I(a)–I(e)], however, shows some interesting differences. For example, peak 1c which contains the final states $(^3P)5p\ ^4D_{3/2}$ and $^2P_{1/2}$, and is the strongest peak of the final states having a ^3P core configuration for the first resonance, has in the second resonance yielded its place to peak $1d[4p^4(^3P)5p\ ^4D_{1/2}, ^2P_{3/2}, ^2D_{5/2}]$. The relative cross sections for transitions to the various final states are apparently dependent on the nature of the resonance and not just the final state.

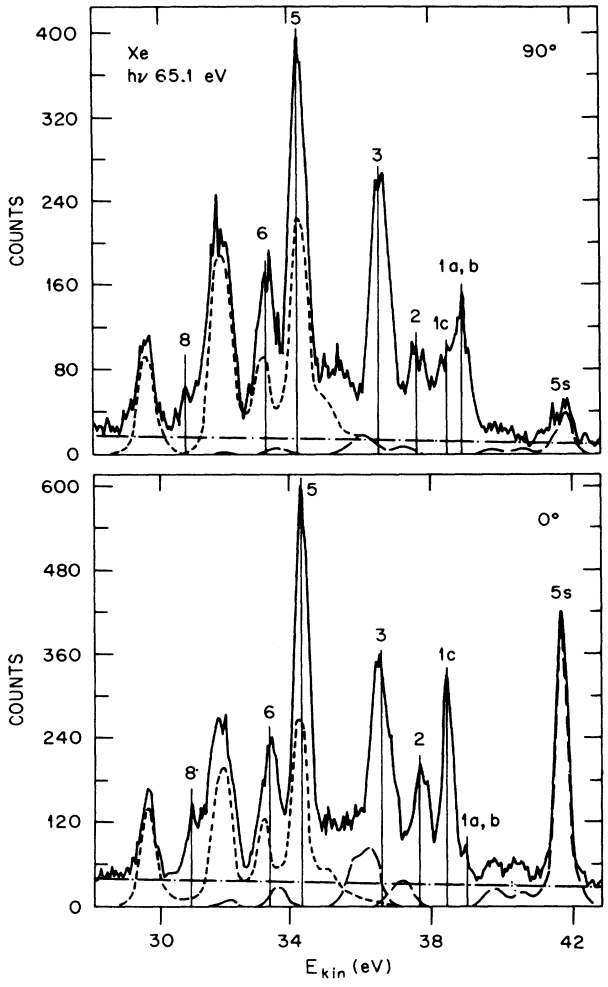

FIG. 5. Electron spectra for xenon measured at a photon energy of 65.1 eV. The kinetic-energy scale is given in eV. The long vertical lines mark the positions where the intensities are measured. See Table III(a) for results of analyses and designation of numbered peaks. The 5s photoelectron peak is so indicated in the figure. Spectra have been taken at $\theta = 90°$ (upper) and 0° (lower). The spectra are given by solid lines and the background by dashed lines: general background, dot dash; satellite structure, long dash; and normal Auger spectra, short dash. The resolution of the photon source is 0.19 eV FWHM and that of the electron spectrometer at 90° is 0.36 eV FWHM.

3. Kr: Third resonance ($3d_{5/2} \rightarrow 6p$)

The third resonance is not completely resolved from the second resonance. Because of the reduction in shielding due to the 6p as compared to the 5p electron, the spectra will occur[11] at slightly lower kinetic energies than the first resonance for the same valence-shell final-state configurations and, of course, an additional 1.23 eV lower than the spectra for the second resonance. To help better evaluate the contributions of the second and third resonances, data were taken at $h\nu = 92.4$ and 92.6 eV with a monochromator resolution of 0.19 eV. The lower energy favors the second resonance while the higher energy favors the third. In this way we determine that the contribution at 92.4 eV in Figs. 3 and 2(b) were dominated by the second resonance. (In any case, peaks 1a–1e are completely unaffected by the third resonance.) Data taken at 92.6 eV showed some possible contribution from the third resonance, but the counting rates were so poor and the background corrections so large that we have chosen not to report any of the results.

4. Kr: Lower kinetic-energy resonant auger processes

Resonant Auger processes involving the 4s valence electrons instead of the 4p subshell result in the ejection of electrons with lower kinetic energy. Results for some of these transitions are found in Tables I(f) and I(g) and Fig. 4. Spectra are examined at both the first and second resonances. The most trenchant generalization that can be made is that the β values tend toward slightly positive values.

B. Xe 4d

As with Kr 3d, a description taken from the literature[19] will be given of the resonance region below the ionization potentials of the Xe 4d core levels. The lowest-resonance energy occurs at 65.11 eV, representing the transition $4d_{5/2} \rightarrow 6p$. The next-higher-energy resonance occurs at 66.38 eV ($4d_{5/2} \rightarrow 7p$). The $4d_{3/2} \rightarrow 6p$ transition or fourth resonance requires 67.04 eV. Close by is the third resonance, $4d_{5/2} \rightarrow 8p$ at 66.85 eV. The relative oscillator strengths are given as 1.0, 0.33, 0.11, and 0.74 for the first four resonances. The ionization potentials for the $4d_{5/2}$ and $4d_{3/2}$ levels are, respectively, 67.55 and 69.54 eV.

1. Xe: First resonance ($4d_{5/2} \rightarrow 6p$)

Results from the study of resonant Auger processes for the first resonance are given in Tables III(a) and III(b) and Figs. 5 and 6. As with Kr the assignments have been made with the help of optical data[20,24] and previous resonant Auger spectroscopy.[2] The numbering of the peaks follows Aksela *et al.*[2] One might expect similarity between the resonant Auger processes for Xe $4d$ and Kr $3d$, and, in fact, such is the case. In the first resonance of both rare gases the highest kinetic-energy peaks ($1a,b$) of Tables I(b) and III(b), show a large negative β followed by a peak with a high positive value ($1c$). The peaks $3a,b$ in Xe for the $5p^4(^1D)6p$ final state, which correspond to the $2a,b$ peaks in Kr, are fairly isotropic, while the $5p^4(^1S)6p$ state, peak 5, for Xe is quite positive which corresponds to peak 5 for Kr. Upon examining the results more closely, it is found that the higher-energy peak $1a$, consists of the final states $^4P_{5/2,3/2}$ just as in Kr so that the theoretical treatment in terms of the angular-momentum transfer theory is the same as with Kr (see Table II and earlier discussion). The penultimate peak, $1b$, has a β value near -1, and from optical data[24] consists of $5p^4(^3P)6p\ ^4P_{1/2}$, $^4D_{7/2,5/2}$. (A more recent analysis of the Xe optical data[24] suggests $^2P_{1/2}$ and $^2D_{5/2}$ rather than the corresponding quartet states.) The peak from Xe designated $1c$ has a high positive value for β. It has been assigned to the $^4D_{3/2}$ final state by Moore[20] but Hansen and Persson[24] suggest $^2P_{3/2}$.

Peak 5 of our Xe study, higher kinetic energy, first resonance, appears to arise principally from the $5p^4(^1S)6p$ final state. This was also the conclusion of Aksela *et al.*

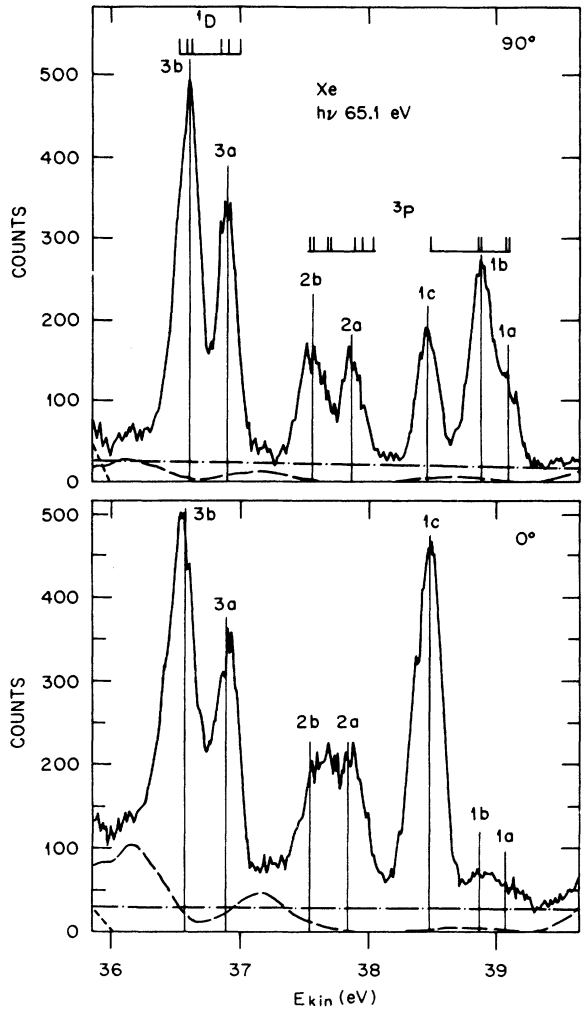

FIG. 6. Details of the higher kinetic-energy portions of the electron spectra for xenon measured at photon energy of 65.1 eV. The kinetic-energy scale is given in eV. The long vertical lines mark the positions where the intensities are measured. See Table III(b) for results of analyses and designation of numbered peaks. Spectra have been taken at $\theta = 90°$ (upper) and 0° (lower). The spectra are given by solid lines and the background by dashed lines: general background, dot dash; satellite structure, long dash; and normal Auger spectra, short dash. The short vertical lines, which indicate possible positions of Auger peaks, are derived from optical data (Ref. 20). The resolution of the photon source is 0.19 eV FWHM and that of the electron spectrometer at 90° is 0.12 eV FWHM.

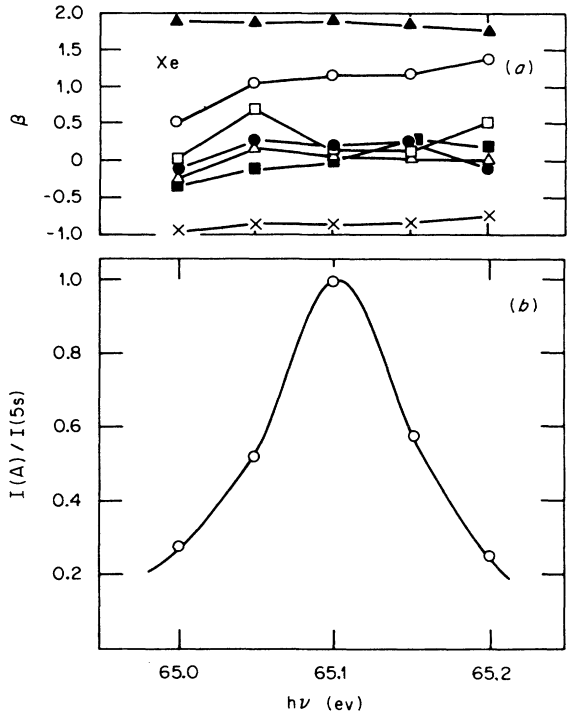

FIG. 7. Plot of the β values and intensity as a function of photon energy going over the first preionization resonance for Xe $4d$. See Fig. 6 and Table III(b) for identification of peaks. In this figure, the numbered peaks are denoted as follows: $X = 1a,b$; $\circ = 1c$; $\square = 2a$; $\triangle = 2b$; $\bullet = 3a$; $\blacksquare = 3b$; and $\blacktriangledown = 5s$ photoelectron peak. The intensity in (b) $[I(A)/I5s]$ corrected to the magic angle is taken as the summed intensities of the resonant Auger peaks (1–3) divided by the intensity of the $5s$ photoelectron peak, which is essentially constant over this energy range. The resolution of the photon source is 0.10 FWHM and that of the electron spectrometer at 90° is 0.24 eV FWHM.

based on their calculations.[2] The high-β value suggests that it has a source similar to peak 4 [$4p^4(^1S)5p$] in Kr (Fig. 1). To complicate the situation, results on the weak resonance at 66.38 eV, not plotted, show three distinct resonant peaks, one of which has about 1.2 eV higher kinetic energy than peak 5 in Fig. 5. A shakeup process during the Auger decay, following the first resonance, would lead to $(4d_{5/2})^{-1}6p \rightarrow (5p)^4 7p$ or the same final state as reached in the second resonance: $(4d_{5/2})^{-1}7p \rightarrow (5p)^4 7p$. The kinetic energy of the latter process would be higher by the difference in energies of the resonance or 1.27 eV. Thus peak 5 could contain a shake-up process. To still further complicate matters, Moore assigns from optical spectroscopy[20] an energy level to the $5p^4(^1S)6p$ state that would give a kinetic energy to the Auger process from the first resonance of 35.60 eV. There is no obviously strong contribution in the resonant Auger spectra at this energy (between peaks 5 and 3 in Fig. 5), although Aksela's data[2] suggest a weak peak in the region. If the assignment of peak 5 is, at least in part, due to $5p^4(^1S)6p$ then the earlier optical assignment[20] must be incorrect. In fact, Hansen and Persson[24] assign new lines to the ^1S state that would result in Auger energies of 34.48 and 34.60 eV, which fit well the experimental peak 5 in Fig. 5. Our data thus confirms the new assignments of Hansen and Persson.

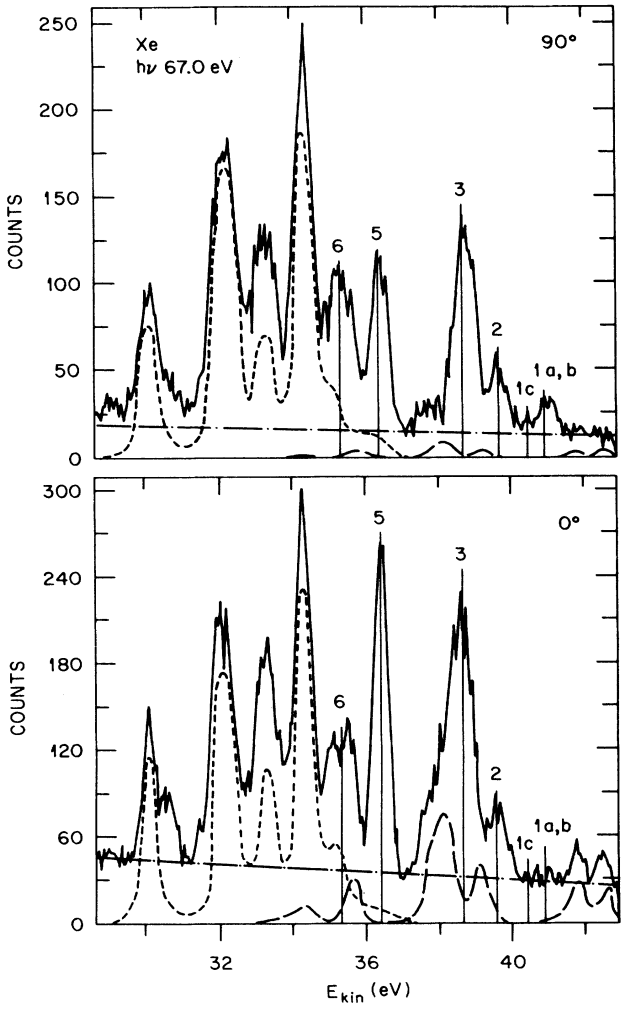

FIG. 8. Electron spectra for xenon measured at a photon energy of 67.0 eV. The kinetic-energy scale is given in eV. The long vertical lines mark the positions where the intensities are measured. See Table III(c) for results of analyses and designation of numbered peaks. The spectra are given by solid lines and the background by dashed lines: general background, dot dash; satellite structure, long dash; and normal Auger spectra, short dash. The resolution of the photon source is 0.19 eV FWHM and that of the electron spectrometer at 90° is 0.36 eV FWHM.

Before consideration of the high kinetic-energy end of the Auger spectrum from the first preionization resonance of Xe $4d$ is completed, results will be discussed concerning the behavior of β as the photon energy is scanned over the resonance. In Fig. 7 are plotted the β values for various resonant Auger peaks as a function of photon energy. Also plotted is the total intensity of the Auger peaks (labeled 1–3) relative to the $5s$ photoelectron peak, which is essentially constant in this energy range. The monochromator resolution was reduced to 0.10 eV. If interchannel coupling or direct photoionization played an important role, one might expect a large oscillation in the β as one passed over the resonance. Little or none is observed within experimental error.

2. *Xe: Fourth resonance ($4d_{3/2} \rightarrow 6p$)*

Results on the fourth resonance for Xe $4d$ are given in Table III(c) and Fig. 8. Contributions from the third resonance $4d_{5/2} \rightarrow 8p$ should not play a role. The third resonance, which is partially resolved from the fourth resonance, has a cross section an order of magnitude lower than the fourth resonance, and the peaks should appear several volts lower in the Auger spectra than those from the fourth resonance. Since the final states of the fourth resonance are the same set as for the first resonance, the β values and intensities should be closely compared. The results are similar except for the highest kinetic-energy peaks. The intensities for both $1a,b$ and $1c$ are much weaker in the case of the resonance from the $4d_{3/2}$ level. The $1c$ peak is particularly weak, and has a β value which is uncertain but no longer strongly positive. Again, there is a marked deviation from what might be expected if one considers only the final states.

3. *Xe: Lower kinetic-energy resonance Auger processes*

Results from the lower kinetic-energy Auger processes involving the $5s$ valence electrons are shown in Fig. 9 and Tables III(d) and III(e). As with the studies on Kr, it is to be noted that β tends toward a more positive value.

C. Ar $2p$

The study of resonant Auger processes in argon differs from Kr and Xe in that the core shell is a p orbital rather

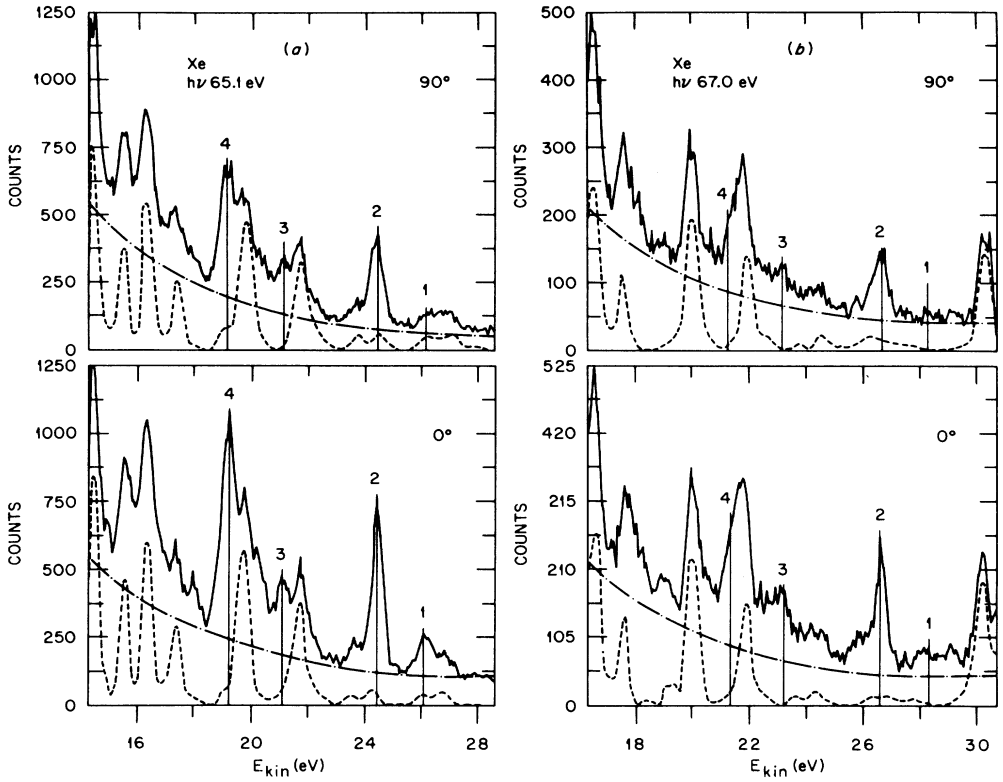

FIG. 9. Comparison of the lower kinetic-energy portion of the electron spectra for xenon measured at (a) 65.1 and (b) 67.0 eV. The long vertical lines mark the positions where intensities are measured. See Tables III(d) and III(e) for results of analyses and designation of numbered peaks. Spectra have been taken at $\theta=90°$ (upper) and 0° (lower) and are drawn as solid lines. The background are given by dashed lines: general background, dot dash; normal Auger spectra, short dash. The kinetic-energy scale is given in eV. The resolution of the photon source is 0.19 eV FWHM and that of the electron spectrometer at 90° is 0.36 eV FWHM.

than a *d* orbital. The first resonance for promoting a $2p$ vacancy in argon occurs[19] at 244.39 eV, which represents the transition $2p_{3/2}\rightarrow 4s$. The second resonance occurs at 246.51 eV ($2p_{1/2}\rightarrow 4s$) and the third resonance, $2p_{3/2}\rightarrow 3d$, requires 246.93 eV. The relative oscillator strengths are 0.51, 0.28, and 1.0 for the first three resonances, respectively. The ionization potentials for the $2p_{3/2}$ and $2p_{1/2}$ core shells are 248.63 and 250.78 eV.

1. *Ar: First resonance ($2p_{3/2}\rightarrow 4s$)*

Results from the resonant Auger spectra due to the first resonance are given in Fig. 10 and Tables IV(a) and IV(b). The assignments have been made with the help of optical data[20] and Aksela's[3] work on Ar $2p$. As with Kr $3d$ and Xe $4d$, the resonant Auger spectrum of Ar $2p$ shows an unusually high negative-β value associated with the high kinetic-energy peaks of the first resonance. Using data from the electron spectra with higher resolution, it has been established that the usually high negative β is due to peak $1b$ or the final state $3p^4(^3P)4s\ ^2P_{3/2,1/2}$. These doublet states contrast with the results on Kr and Xe in which the quartet final states give rise to the parity-unfavored transitions. Angular-momentum transfer theory suggests that changes should occur [see Eqs. (4a) and (4b)]. In Ar $2p$ the first resonance is to a $4s$ state making the parity of the final state positive, thus reversing the criteria for favored versus unfavored transitions. From angular momentum transfer theory when *LS* coupling is used for argon, it is predicted that the ^2P state will be parity unfavored (Table II). As can be seen from the experimental results for peaks $1b$, 2, and 3 from Fig. 10, and Table IV(b), the predictions of Table II are borne out. That is, the ^2P final state, which is unfavored has a high negative-β value, while the ^2D and ^2S final states, which are favored, have positive-β values. As noted earlier this result can be obtained using the alignment parameter from normal Auger theory.

It has been established that with Auger processes the basic form of Eq. (1) is valid.[13,25] That is, the angular distribution has a $\cos^2\theta$ dependence. The angular dependence was checked experimentally for peaks 1 (^3P) and 2 (^1D) of the first resonant Auger process of Ar $2p$ as well as for $3s$ photoelectrons by varying the angle θ. The data were all consistent within experimental error with a $\cos^2\theta$ dependence. That is, the large negative β's observed in this paper do not presuppose any other behavior than the usual dipole excitation.

2. *Ar: Higher-energy resonance ($2p_{1/2}\rightarrow 4s$; $2p_{3/2}\rightarrow 3d$)*

The second and third resonances for Ar $2p$ are not resolvable due to monochromator limitations at the

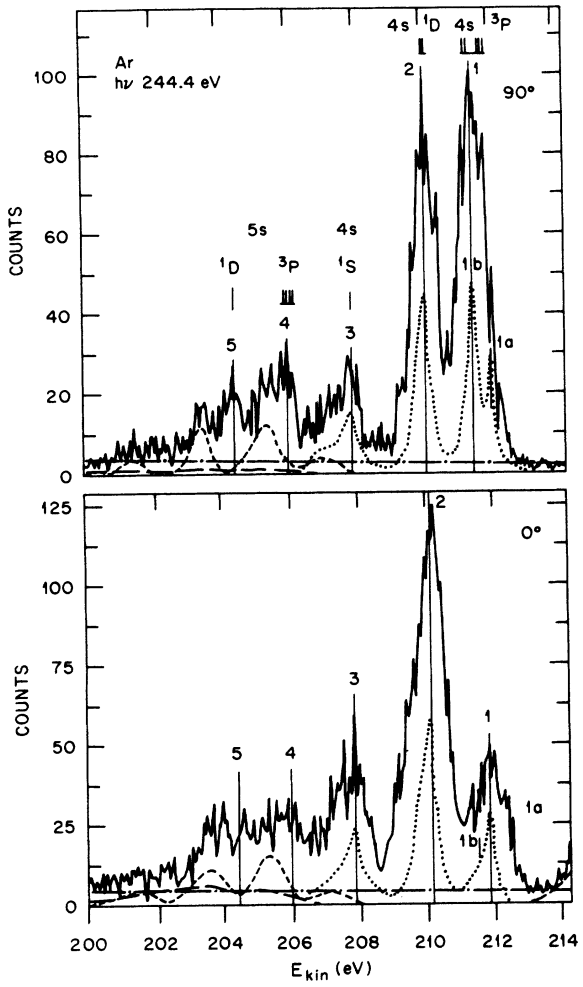

FIG. 10. Electron spectra for argon measured at a photon energy of 244.4 eV. The kinetic-energy scale is in eV. The long vertical lines mark the positions where the intensities are measured. See Table IV(a) and IV(b) for results of analyses and designation of numbered peaks. Spectra have been taken at $\theta=90°$ (upper) and 0° (lower). The spectra are given by solid lines and the background by dashed lines: general background, dot dash; satellite structure, long dash; and normal Auger spectra, short dash. The short vertical lines, which indicate possible positions of Auger peaks, are derived from optical data (Ref. 20). Results from a run having a better electron resolution are shown as dotted lines, which illustrate the separation into peaks 1*a* and 1*b*. For the spectra shown by the solid lines, the resolution of the photon source is 1.30 eV FWHM and that of the electron spectrometer at 90° is 0.60 eV FWHM. For the spectra shown by the dotted lines the resolution of the photon source is 1.82 eV FWHM and that of the electron spectrometer at 90° is 0.36 eV FWHM.

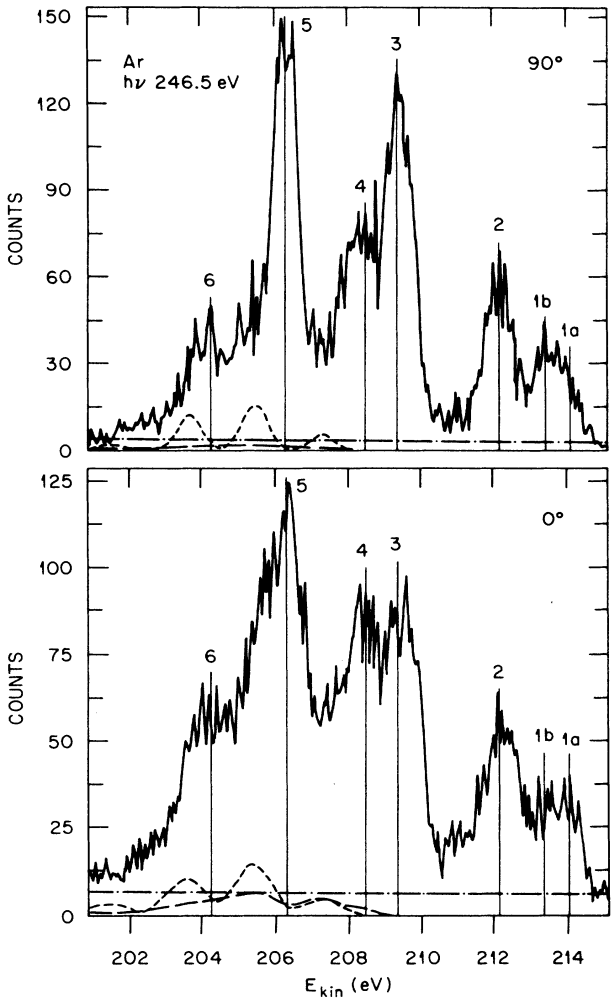

FIG. 11. Electron spectra for argon measured at a photon energy of 246.5 eV. The kinetic-energy scale is in eV. The long vertical lines mark the position whre the intensities are measured. See Table IV(c) for results of analyses and designation of numbered peaks. Spectra have been taken at $\theta=90°$ (upper) and 0° (lower). The spectra are given by solid lines and the background by dashed lines: general background, dot dash; satellite structure, long dash; and normal Auger spectra, short dash. The resolution of the photon source is 1.30 eV FWHM and that of the electron spectrometer at 90° is 0.60 eV FWHM.

high-photon energy required. Thus, in Fig. 11 and Table IV(c), one finds peaks assigned to both resonances. One can compare peaks 1 and 2 with those obtained from the first resonance [Fig. 10 and Table IV(a)] since both processes have the same final states. It does appear that, considering the limited resolution available, peak 1*b* of the second resonance also possesses a sizable negative β similar to that discussed for the first resonance. Aksela *et al.*[3] have assigned peaks 4–6 to shakeup phenomena and these peaks are quite intense. The only remarks that might be made regarding the β parameters for the higher resonances of Ar 2*p* is that they tend towards a negative value.

D. Normal Auger processes

For comparison with the resonant Auger processes, results for the normal Auger processes have been listed in Tables I(h), III(f), III(g), and IV(d) for photoionization of the Kr 3*d*, Xe 4*d*, and Ar 2*p* core shells. The assignments

are those reported by Aksela *et al.*[1-3] In contrast to the resonant Auger processes, the normal Auger processes show rather isotropic behavior. There are three possible reasons for this generalization. First, the resonance condition may enhance unfavored transitions, which, under conditions of off resonance, are unimportant. Second, there is a leveling process in the normal Auger process caused by having two electrons carry away angular momentum. Third, in the resonant process there are at least two open shells, the partially emptied valence shell and the resonantly excited single-electron state, whose interactions can give rise to a wide variety of different final states.

IV. CONCLUSION

This paper demonstrates the importance of coupling high-electron resolution with angle-resolved studies of resonant Auger processes. In particular, it has been observed in spectra derived from resonances below the ionization thresholds of Kr $3d$, Xe $4d$, and Ar $2p$ that peaks in the higher kinetic-energy region of the Auger spectra have angular distribution parameters β close to the extreme value of -1. Angular momentum transfer theory has been used as a framework for discussing the unusual degree of angular anisotropy observed here. This approach suggests transitions of unfavored parity to explain the negative-β values. Another approach using the alignment parameter from normal Auger theory has not been thoroughly investigated, but has been shown to lead to the correct result when applied to argon assuming LS coupling. Both of these approaches as discussed in this paper use either the LS or jj coupling scheme, rather than a more appropriate intermediate coupling. Explicit calculations are needed to fully understand the range of β values observed.

In addition to a more complete understanding of the nature of photoelectron dynamics, angle-resolved, high-resolution resonant Auger spectroscopy can be useful for supplementing optical spectroscopy, especially if angular data can help to identify the processes.

ACKNOWLEDGMENTS

This research has been sponsored by the Division of Chemical Sciences, Office of Basic Energy Sciences, U.S. Department of Energy under Contract No. DE-AC05-84OR21400 with Martin Marietta Energy Systems, Inc. Synchrotron radiation was supplied at the Synchrotron Radiation Center, Stoughton, Wisconsin, which is operated under National Science Foundation (NSF) Grant No. DMR 8601349. Research at the University of Wisconsin was supported by a grant from the General Motors Corporation. D.R.M. wishes to acknowledge support from the Post Graduate Research Training Program under Contract No. DE-AC05-76OR00033 between the U.S. Department of Energy and Oak Ridge Associated Universities.

[1]H. Aksela, S. Aksela, H. Pulkkinen, G. M. Bancroft, and K. H. Tan, Phys. Rev. A **33**, 3876 (1986).

[2]H. Aksela, S. Aksela, G. M. Bancroft, K. H. Tan, and H. Pulkkinen, Phys. Rev. A **33**, 3867 (1986).

[3]H. Aksela, S. Aksela, H. Pulkkinen, G. M. Bancroft, and K. H. Tan, Phys. Rev. A **37**, 1798 (1988).

[4]D. W. Lindle, P. A. Heiman, T. A. Ferrett, M. N. Piancastelli, and D. A. Shirley, Phys. Rev. A **35**, 4605 (1987).

[5]W. Eberhardt, G. Kalkoffen, and C. Kung, Phys. Rev. Lett. **41**, 156 (1978).

[6]T. A. Carlson, D. R. Mullins, C. E. Beall, B. W. Yates, J. W. Taylor, D. W. Lindle, B. P. Pullen, and F. A. Grimm, Phys. Rev. Lett. **60**, 1382 (1988).

[7]S. Aksela, O. P. Sairanen, H. Aksela, G. M. Bancroft, and K. H. Tan, Phys. Rev. A **37**, 2934 (1988); S. Aksela, K. H. Tan, H. Aksela, and G. M. Bancroft, *ibid.* **33**, 258 (1986); W. Eberhardt, J. Stöhr, J. Feldhaus, E. W. Plummer, and F. Sette, Phys. Rev. Lett. **51**, 2370 (1983); W. Eberhardt, E. W. Plummer, C. T. Chen, and W. K. Ford, Aust. J. Phys. **39**, 853 (1986).

[8]G. G. B. de Souza, P. Morin, and I. Nenner, Phys. Rev. A **34**, 4770 (1986); J. Chem. Phys. **83**, 492 (1985).

[9]T. A. Ferret, D. W. Lindle, P. A. Heiman, H. G. Kerkhoff, U. E. Becker, and D. A. Shirley, Phys. Rev. A **38**, 1916 (1986); C. M. Truesdale, D. W. Lindle, P. H. Kobrin, U. E. Becker, H. G. Kerkhoff, P. A. Heiman, T. A. Ferrett, and D. A. Shirley, J. Chem. Phys. **80**, 2319 (1984); D. W. Lindle, C. M. Truesdale, P. H. Kobrin, T. A. Ferrett, P. A. Heiman, U. Becker, H. G. Kerkhoff, and D. A. Shirley, *ibid.* **81**, 5375 (1984).

[10]H. Kanamori, S. Iwata, A. Mikuni, and T. Sasaki, J. Phys. B **17**, 258 (1986).

[11]T. A. Carlson, P. Gerard, M. O. Krause, G. Von Wald, J. W. Taylor, F. A. Grimm, and B. P. Pullen, J. Electron. Spectrosc. **47**, 227 (1988).

[12]These expressions can be extracted for any standard text, e.g., M. O. Krause, in *Synchrotron Radiation Research,* edited by H. Winick and S. Doniach (Plenum, New York, 1980), Chap. 5.

[13]U. Fano and D. Dill, Phys. Rev. A **6**, 185 (1972); D. Dill, *ibid.* **7**, 1976 (1973).

[14]W. Mehlhorn, in *X-Ray and Atomic Inner-Shell Physics–1982,* edited by B. Crasemann, AIP Conference Proceedings No. 94 (AIP, New York, 1982), p. 53.

[15]E. G. Berezhko and N. M. Kabachnik, J. Phys. B **10**, 2467 (1977).

[16]N. M. Kabachnik, I. S. Lee, and O. V. Lee, Vol. 294 of *Lecture Notes in Physics,* edited by D. Berényi and G. Hock (Springer-Verlag, 1988), p. 220ff.

[17]M. O. Krause, T. A. Carlson, and P. R. Woodruff, Phys. Rev. A **24**, 1374 (1981).

[18]S. H. Southworth, U. Becker, C. M. Truesdale, P. H. Kobrin, D. W. Lindle, S. Owaki, and D. A. Shirley, Phys. Rev. A **28**, 261 (1983); S. H. Southworth, P. H. Kobrin, C. M. Truesdale, D. Lindle, S. Owaki, and D. H. Shirley, *ibid.* **24**, 2257 (1981).

[19]P. A. Heimann, D. W. Lindle, T. A. Ferrett, S. H. Liu, L. J. Mebhurst, M. N. Piancastelli, D. A. Shirley, U. Becker, H. G. Kerkhoff, B. Langer, D. Szostak, and R. Wehlitz, J. Phys. B **20**, 5005 (1987).

[20]C. E. Moore, *Atomic Energy Levels,* Natl. Bur. Stand. (U.S.), Circ. No. 467 (U.S. GPO, Washington, D.C., 1952), Vols. I–III.

[21]C. D. Caldwell, M. O. Krause, and J. Jimenéz-Mier, Phys. Rev. A **37**, 2408 (1988).

[22]S. T. Manson and A. F. Starace, Rev. Mod. Phys. **54**, 389 (1982). Using the notation in this reference $\vec{j}_t=\vec{J}_c+\vec{S}-\vec{J}_0$, where $J_0=0$ for the ground state of neutral Ar, Kr, or Xe.

[23]D. Dill, *Photoionization and Other Probes of Many-Electron Interactions, Series B: Physics,* edited by F. J. Wuilleumier (Plenum, New York, 1976), p. 387.

[24]J. E. Hansen and W. Persson, Phys. Scr. **36**, 602 (1987).

[25]Reference 14, p. 53.